Title

The first DEP domain of the RhoGEF P-Rex1 autoinhibits activity and contributes to membrane binding.

Journal

Journal of Biological Chemistry, 295(36)

Authors

Ravala, Sandeep

Hopkins, Jesse

Plescia, Caroline

et al.

Publication Date

2020-09-04

DOI

10.1074/jbc.RA120.014534

The first DEP domain of the RhoGEF P-Rex1 autoinhibits activity and contributes to membrane binding

Received for publication, May 25, 2020, and in revised form, July 8, 2020 Published, Papers in Press, July 13, 2020, DOI 10.1074/jbc.RA120.014534

Sandeep K. Ravala[1,2], Jesse B. Hopkins[3], Caroline B. Plescia[2], Samantha R. Allgood[1], Madison A. Kane[4], Jennifer N. Cash[5], Robert V. Stahelin[2], and John J. G. Tesmer[1,2,*]

From the Departments of [1]Biological Sciences and [2]Medicinal Chemistry and Molecular Pharmacology, Purdue University, West Lafayette, Indiana, USA, the [3]Biophysics Collaborative Access Team, Illinois Institute of Technology, Advanced Photon Source, Argonne National Laboratory, Lemont, Illinois, USA, the [4]College of Engineering, California State University, Long Beach, California, USA, and the [5]Department of Biological Chemistry & Life Sciences Institute, University of Michigan, Ann Arbor, Michigan, USA

Edited by Henrik G. Dohlman

Phosphatidylinositol (3,4,5)-trisphosphate (PIP_3)-dependent Rac exchanger 1 (P-Rex1) catalyzes the exchange of GDP for GTP on Rac GTPases, thereby triggering changes in the actin cytoskeleton and in transcription. Its overexpression is highly correlated with the metastasis of certain cancers. P-Rex1 recruitment to the plasma membrane and its activity are regulated via interactions with heterotrimeric G$\beta\gamma$ subunits, PIP_3, and protein kinase A (PKA). Deletion analysis has further shown that domains C-terminal to its catalytic Dbl homology (DH) domain confer autoinhibition. Among these, the first dishevelled, Egl-10, and pleckstrin domain (DEP1) remains to be structurally characterized. DEP1 also harbors the primary PKA phosphorylation site, suggesting that an improved understanding of this region could substantially increase our knowledge of P-Rex1 signaling and open the door to new selective chemotherapeutics. Here we show that the DEP1 domain alone can autoinhibit activity in context of the DH/PH-DEP1 fragment of P-Rex1 and interacts with the DH/PH domains in solution. The 3.1 Å crystal structure of DEP1 features a domain swap, similar to that observed previously in the Dvl2 DEP domain, involving an exposed basic loop that contains the PKA site. Using purified proteins, we show that although DEP1 phosphorylation has no effect on the activity or solution conformation of the DH/PH-DEP1 fragment, it inhibits binding of the DEP1 domain to liposomes containing phosphatidic acid. Thus, we propose that PKA phosphorylation of the DEP1 domain hampers P-Rex1 binding to negatively charged membranes in cells, freeing the DEP1 domain to associate with and inhibit the DH/PH module.

The diffuse B cell lymphoma (Dbl) family of guanine nucleotide exchange factors (GEFs) (1) has ~70 members featuring one or more Dbl homology (DH) domains, which catalyze nucleotide exchange on Rho GTPases. The DH domain is almost always followed by a pleckstrin homology (PH) domain to form a DH/PH module (2). The PH domains in Dbl RhoGEFs can bind to phospholipids and help in membrane translocation, as in Dbs, Tiam, and Lfc (3–5), or interact with other proteins, as in TrioN and p63RhoGEF (6, 7), or directly regulate the binding of GTPases to the adjacent DH domain as in Dbs, LARG, and TrioC (8–10). In each RhoGEF, other domains are present that can impose additional layers of regulation on GEF activity. These domains are known to interact with lipids, cofactors, other cellular/membrane proteins, or directly with the DH domain of the enzyme (3). For example, the Src-homology 3 (SH3) domain of ASEF interacts with both of its DH and PH domains to obstruct binding and activation of CDC42 (11).

Phosphatidylinositol (3,4,5)-trisphosphate (PIP_3)-dependent Rac exchanger 1 (P-Rex1) is an unusually large Dbl RhoGEF expressed in neutrophils that catalyzes nucleotide exchange on Rac GTPases (12). Its N-terminal DH/PH domains are followed by two DEP domains (DEP1 and DEP2), two PDZ domains (PDZ1 and PDZ2), and a large C-terminal domain with homology to inositol polyphosphate-4-phosphatase (IP4P) domains (Fig. 1*A*) (12, 13). P-Rex1 is a downstream effector of both G_i and G_s coupled G protein–coupled receptors (GPCRs) by virtue of its synergistic activation by G$\beta\gamma$ and PIP_3 (12) and its regulation by protein kinase A (PKA) (14–17). P-Rex1 in normal cells mediates chemotaxis (18–20), but it is overexpressed in metastasizing cancers (21–23) and other studies show its involvement in neurological disorders (24), inflammatory diseases (25), and type 2 diabetes (26, 27). Thus, P-Rex1 represents an important therapeutic target, and understanding its atomic structure and mechanisms of regulation would facilitate the drug discovery process.

In its basal state, P-Rex1 is autoinhibited and localized in the cytoplasm (12). Deletion of domains C-terminal to the DH domain in the full-length enzyme, including the PH domain, generally led to increased GEF activity, thereby implying involvement of these domains in autoinhibition (28). These studies also showed that the DH/PH fragment of P-Rex1 has significantly higher activity than P-Rex1. Thus, the PH domain does not seem to inhibit GEF activity on its own, implying coordination among the C-terminal domains in autoinhibition.

The P-Rex1 PH domain mediates binding and activation by PIP_3, and also contains a β3-β4 polybasic loop, which might play a role in interacting with the cell membrane through ionic interactions (29). Our recent single particle cryo-EM structure of P-Rex1 in complex with G$\beta\gamma$ resolved the C-terminal portion of the protein spanning from the DEP2 domain through the C terminus (13), wherein the DEP2, PDZ1, PDZ2, and IP4P domains coalesce to form a G$\beta\gamma$ interaction scaffold. The DH/

This article contains supporting information.

* For correspondence: John J.G. Tesmer, jtesmer@purdue.edu.

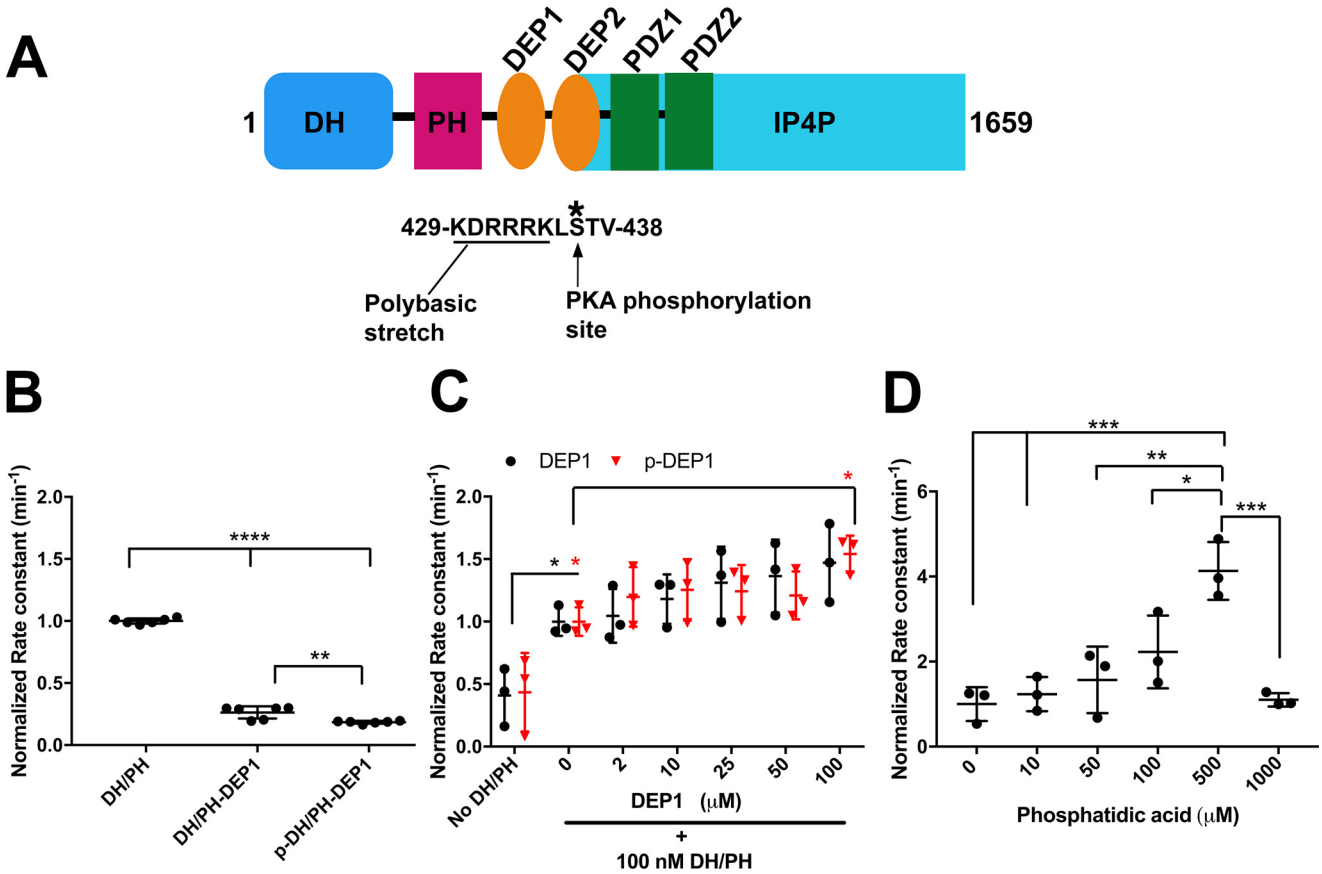

Figure 1. The P-Rex1 DEP1 domain inhibits GEF activity. *A,* domain architecture of full-length P-Rex1. P-Rex1 protein has a DH/PH catalytic module at its N terminus followed by two DEP domains, two PDZ domains, and a C-terminal IP4P domain. The IP4P domain interacts with DEP2 and both PDZ domains. The DEP1 domain (residues 409-499) has a polybasic stretch of residues in which is found a consensus PKA phosphorylation site at Ser-436. *B,* activities of DH/PH, DH/PH-DEP1 and *p*-DH/PH-DEP1 measured in a FRET-based assay by monitoring the dissociation of mant-GDP from unprenylated Cdc42 in the absence of liposomes. GEF activity was normalized to that of DH/PH. ****, $p < 0.0001$, **, $p = 0.0018$. *C,* GEF activity of the P-Rex1 DH/PH fragment (100 nM) was assessed after addition of increasing amounts of DEP1 or *p*-DEP1 (0-100 μM) in the absence of liposomes. GEF activity was normalized to that of DH/PH in the absence of DEP1. *, $p < 0.0460$ for DH/PH *versus* DEP1, $p < 0.0299$ for DH/PH *versus* pDEP1, and $p < 0.0388$ for DH/PH plus 100 μM pDEP1 *versus* DH/PH. *D,* GEF activity of DH/PH-DEP1 was assayed in liposomes containing increasing concentrations of PA (0-1000 μM). Control liposomes contained 50% (w/w) mol each of POPC and POPE. All other liposomes had an increasing mol % of PA: 10 μM (1 mol %), 50 μM (5 mol %), 100 μM (10 mol %), 500 μM (50 mol %), and 1000 μM (100 mol %). Addition of PA was compensated with decreasing POPE concentration with the exception of 1000 μM, wherein the liposomes are 100% PA. GEF activity was normalized to that of DH/PH-DEP1 in control liposome. ***, $p = 0.0004$ for DH/PH-DEP1 plus control liposome with no PA *versus* DH/PH-DEP1 plus liposome with 500 μM PA, ***, $p = 0.0008$ for DH/PH-DEP1 plus liposome with 10 μM PA *versus* DH/PH-DEP1 plus liposome with 500 μM PA, ***, $p = 0.0005$ for DH/PH-DEP1 plus liposome with 500 μM PA *versus* DH/PH-DEP1 plus liposome with 1000 μM PA, **, $p = 0.0022$, and *, $p = 0.0202$. In each graph, data are from at least three independent experiments measured in duplicate, with *error bars* representing the mean ± S.D.

PH-DEP1 domains were disordered in the structure. Because the DH/PH domains exhibit robust basal activity on their own, autoinhibition would seem to be imposed by DEP1, the C-terminal G$\beta\gamma$-binding assembly, or both. Furthermore, Ser-436 in the DEP1 domain is phosphorylated by PKA, which blunts activation by G$\beta\gamma$ and PIP_3 (14–16). The DEP1 domain is also reported to contribute to a binding site for mTOR, which positively regulates P-Rex1 signaling (30).

Therefore, the DEP1 domain seems poised to play a key role in regulating the GEF activity of P-Rex1. To gain further insight, we determined its crystal structure and compared the activity and the solution structures of the DH/PH and DH/PH-DEP1 fragments of P-Rex1. We also studied the effect of PKA phosphorylation on the GEF activity and solution conformation of the DH/PH-DEP1 fragment. We further tested if PKA phosphorylation affects the ability of the domain to bind liposomes. Our results support a model in which the DEP1 domain associates with and inhibits the DH/PH module in a phosphorylation-independent manner, at least *in vitro*. However, because phosphorylation by PKA diminishes the ability of the DEP1 domain to bind negatively charged phospholipids, it implies that PKA phosphorylated P-Rex1 will lose its ability to efficiently interact with cellular membranes, which will diminish its interactions with other membrane associated regulators such as PIP_3 and G$\beta\gamma$.

Results

The P-Rex1 DEP1 domain inhibits GEF activity

In a previous study (28), deletion of both DEP domains in P-Rex1 led to an increase in basal activity. In another study, it was shown that fragments of P-Rex1 that included the tandem DEP and tandem PDZ domains had less activity in cells than the DH/PH module alone (15). Because our recent structure showed that DEP2 is intimately incorporated into the G$\beta\gamma$-binding module (13), we hypothesized that the DEP1 domain

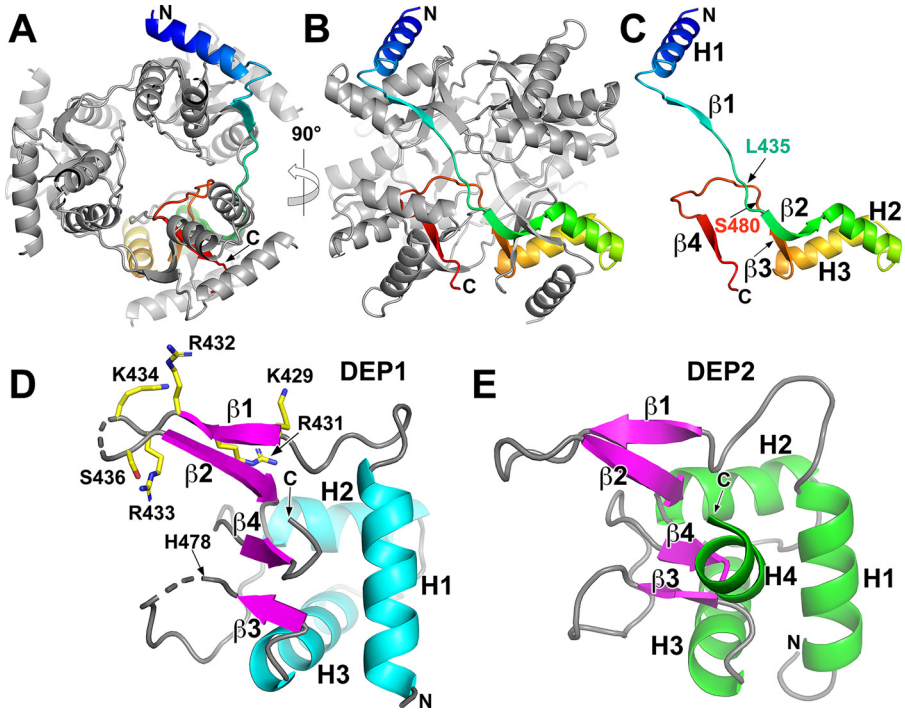

Figure 2. Crystal structure of the P-Rex1 DEP1 domain. Although there is only one DEP1 chain per asymmetric unit, it crystallized as a double domain-swapped D_3 hexamer, in which each DEP1 chain contributes to three different protomers. *A*, top view of the DEP1 hexamer along the 3-fold symmetry axis. The unique DEP1 chain is colored with a gradient from its N (*blue*) to C (*red*) terminus. *B*, the hexamer rotated 90° around a vertical axis relative to *A* so the view is down the dihedral 2-fold axis. The unique DEP1 chain can be seen here contributing to the *top left*, then the *bottom right*, and finally the *bottom left protomer*. *C*, the unique chain of DEP1 from *B* with the approximate positions corresponding to the two domain swaps indicated. *D*, cartoon representation of the deconvoluted DEP1 structure, with domain-swapped loops indicated by *dashed lines*. Positively charged residues and Ser-436 in its polybasic β hairpin loop are shown with stick models for side chains. *E*, cartoon representation of P-Rex1 DEP2 domain from PDB entry 6PCV, which is the most closely related DEP domain structure to DEP1. It contains an extra helix at the C terminus.

alone could exhibit autoinhibition. Indeed, the GEF activity of DH/PH was 4-fold higher than that of DH/PH-DEP1 (Fig. 1*B*). We next tested whether DEP1 could inhibit the DH/PH domain in *trans* by adding increasing amounts of the independently purified DEP1 domain to the DH/PH module. Surprisingly, instead of the expected decrease in activity of DH/PH, a slight increase was observed (Fig. 1*C*). Thus, either the DEP1 domain binds but does not directly block GTPase binding to the DH domain, or its affinity is too low when not covalently attached to the DH/PH module. In support of the latter hypothesis, there is no observed association of the DEP1 domain with DH/PH by size exclusion chromatography (SEC) (data not shown).

Structure of the P-Rex1 DEP1 domain

The human P-Rex1 DEP1 domain, encompassing residues 409-499, crystallized as a D_3 hexamer wherein each protomer undergoes two domain swaps (Fig. 2, *A–C*). Thus, one unique chain of DEP1 contributes to three different DEP domains in the hexamer. DEP1 is predominantly monomeric in solution (Fig. S2*A*) but does exhibit evidence of some dimers and tetramers. The domain swaps in the DEP1 structure occur at residue 435, at the end of what would have been a β hairpin, and at residue 480, before the final β strand of the domain (Fig. 2*C*). Thus, the N and C termini of the DEP1 domain must exhibit a high degree of structural dynamics in solution. Notably, the DEP domain of human Dvl2 also forms a similar domain swap involving the β1–β2 hairpin (31), and consequently it may represent a common occurrence in this domain-fold.

When the domain swaps are deconvoluted (Fig. 2*D*), DEP1 assumes the expected globular DEP-fold with a three-helix bundle (H1–H3), an extended β hairpin formed by β1 and β2 (residues 429-440) between H1 and H2 and ending with two more β strands (β3 and β4) (Fig. 2*D*). Its fold is most closely related to that of the adjacent DEP2 domain (root mean squared deviation of 1.1 Å for 62 Cα atoms) (Fig. 2*E*), with the most variable regions being the domain-swapped loops and an extra C-terminal helix in DEP2. The β1–β2 hairpin projects outward from the core and is extremely basic in character (Fig. 2*D*), in that it contains two lysine and three arginine residues. In other DEP domains, this loop is involved in interactions with negatively charged membranes (32, 33). The loop also happens to be the site of PKA phosphorylation (Ser-436) (15).

The DH/PH-DEP1 fragment adopts a compact shape in solution

Because crystallographic analysis of DH/PH-DEP1 has not yet been successful, we compared the small angle X-ray scattering (SAXS) profiles of the purified DH/PH and DH/PH-DEP1 proteins after SEC (SEC-SAXS) (Fig. 3, *A–B*). In SEC, proteins showed monodisperse elution profiles (Fig. S3, *A* and *B*), and Guinier analysis of the SAXS data (Fig. S4, *A* and *B*) confirmed that the scattering profiles were monodisperse with little or no aggregation. The Guinier fit provided the radius of gyration

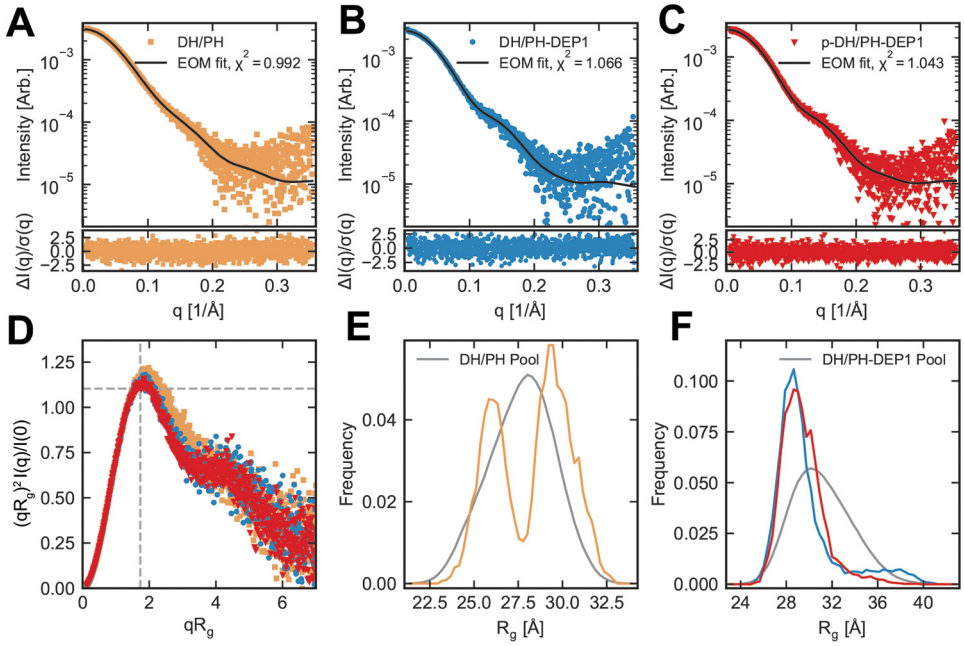

Figure 3. SAXS analysis indicates that the DEP1 domain forms a compact assembly with the DH/PH domains. *A–C*, SAXS data (*points*) and EOM fit (*line*) for DH/PH, DH/PH-DEP1, and *p*-DH/PH-DEP1, respectively. Normalized fit residual is shown in the *bottom panel* of each. *D*, dimensionless Kratky plot for DH/PH (*orange*, *square*), DH/PH-DEP1 (*blue*, *circle*), and *p*-DH/PH-DEP1 (*red*, *triangle*). There is no significant change in shape between the DH/PH-DEP1 and *p*-DH/PH-DEP1 curves, suggesting that they have the same shape. DH/PH has a different shape. All three curves are nongaussian, indicating some flexibility or extended conformations. *E*, EOM results showing the pool (*gray*) and the selected ensemble R_g values for the DH/PH data set. This indicates that DH/PH adopts both compact and extended conformations, relative to all possible conformations. *F*, EOM results showing the pool (*gray*) and the selected ensemble R_g values for the DH/PH-DEP1 (*blue*) and *p*-DH/PH-DEP1 (*red*) datasets. This indicates that DH/PH-DEP1 adopts a relatively compact conformation in solution relative to all possible conformations.

(R_g) and scattering at zero angle ($I(0)$). DH/PH and DH/PH-DEP1 have R_g values of 28.4 ± 0.09 and 29.9 ± 0.09 Å, respectively. The molecular weight calculated from the Guinier fit via the volume of correlation (34), the most appropriate method for flexible systems, was 47 and 59 kDa, respectively, in reasonable agreement with their expected molecular weights (43 and 54 kDa, respectively).

The dimensionless Kratky plot showed a shift in the maximum away from that of a globular protein and an extended tail at higher qR_g (Fig. 3*D*). This indicates some degree of flexibility (35). Pair distribution function (P(r)) analyses of scattering data computed the maximum intramolecular dimensions (D_{max}) of protein molecules, with values of ~105 and 104 Å, for DH/PH and DH/PH-DEP1, respectively (Fig. S5). The maximum interatomic vector in the structure of the DH/PH domain of P-Rex1 (29) is on the order of 100 Å. The fact that DEP1 does not extend this length is consistent with a relatively condensed state for these three domains in solution.

To assess the conformational distribution in solution, we employed ensemble optimization method (EOM) analysis (36). The selected ensemble for DH/PH fits the data very well (Fig. 3*A*), χ^2 = 1.0, and consists of both compact and elongated conformations in solution (Fig. 3*E*, Fig. S6*A*). The selected ensemble is quite different from the generated pool, suggesting that although the system is flexible in solution, it is not adopting purely random configurations. For DH/PH-DEP1, the selected ensembles had χ^2 = 1.1 (Fig. 3*B*). The conformational distribution of DH/PH-DEP1 shows predominantly one set of conformations, concentrated near an R_g of 29 Å and D_{max} of 90 Å (Fig. 3*F* and Fig. S6*B*). This selected ensemble is significantly less extended than the full generated pool, suggesting that DH/PH-DEP1, although flexible, adopts predominantly compact states in solution. This compact state is similar in size to the DH/PH compact state, with R_g and D_{max} peaking at ~26 and ~85 Å, respectively.

The quantitative measure of flexibility of the selected ensembles is given by two metrics R_{flex} and R_σ. R_{flex} of a system can vary from completely flexible (100%) to perfectly rigid (0%). The importance of R_{flex} is not the absolute value, but the value of the selected ensemble relative to the entire pool. R_σ is the ratio of the variance between the selected ensemble and the full ensemble pool. As shown in Table 1, the R_{flex} value of DH/PH is close to that of the ensemble pool, indicating that this protein is very flexible. The R_{flex} of DH/PH-DEP1 is smaller than that of the pool, indicating less flexibility in the system. In both cases, the R_σ is greater than 1. An R_σ greater than 1 can indicate poor quality data (36). Given the high signal to noise and good fit to the data, as indicated by both the χ^2 values and the normalized residuals (Fig. 3, *A* and *B*), this is not the case here. Rather, the large values of R_σ comes from the long tails of the DH/PH-DEP1 and the bimodal distribution of the DH/PH ensemble sizes (such as seen in the R_g plot in Fig. 3, *E* and *F*).

PKA phosphorylation does not affect GEF activity or SAXS properties of the DH/PH-DEP1 fragment

We hypothesized that PKA phosphorylation might augment the ability of the DEP1 domain to inhibit the DH/PH module, as suggested by others previously (15), and that this could lead to a change in their configuration detectable by SAXS. To test these ideas, we first phosphorylated DH/PH-DEP1 (*p*-DH/PH-DEP1) by incubating the protein with PKA and MgATP. After

Table 1
SAXS parameters

	DH/PH	DH/PH-DEP1	*p*-DH/PH-DEP1
Guinier analysis			
$I(0)^a$	0.003 ± 4.8E-06	0.0027 ± 0.00013	0.0027 ± 3.4E-06
R_g (nm)	2.84 ± 0.009	2.99 ± 0.009	2.96 ± 0.007
Q_{min} (nm^{-1})	0.043	0.043	0.043
Q_{max} (nm^{-1})	0.430	0.422	0.433
P(r) analysis			
D_{max} (nm)	10.5	10.4	10.5
Volume (nm^3)	95.2	118	117
MM_{exp} (MM_{cal}) (kDa)	47 (43)	59 (53.7)	59 (53.7)
EOM analysis			
Crystal structure	5FI1	5FI1 and 6VSK	5FI1 and 6VSK
q-Range for fitting (nm^{-1})	0.043-3.55	0.043-3.55	0.043-3.55
Symmetry assumptions	None	None	None
χ^2	1.0	1.1	1.0
Constant subtraction	0.0	0.0	0.0
No. of representative models	3	5	4
Ensemble (pool) average R_g (nm)	2.8 (2.8)	3.0 (3.1)	3.0 (3.1)
Ensemble (pool) average D_{max} (nm)	9.9 (9.0)	10. (10.)	10. (10.)
Ensemble (pool) average volume (nm^3)	83 (79)	104 (102)	103 (102)
Ensemble (pool) average Cα(N)-Cα(C) distance (nm)	7.2 (6.0)	6.3 (6.8)	6.4 (6.8)
R_{flex} ensemble (pool)	86% (87%)	77% (84%)	73% (84%)
R_σ	6.0	4.5	3.4

[a] $I(0)$, R_g, D_{max}, Q_{min}, Q_{max}, MM_{exp}, MM_{cal}, χ^2, R_{flex}, and R_σ are the experimentally determined intensity at zero scattering angle, radius of gyration, maximum particle dimension in the Guinier fit, minimum scattering angle in the Guinier fit, maximum scattering angle, molecular mass calculated from scattering data, molecular mass based on amino acid sequence, χ squared fit between the theoretical scattering of selected ensemble and the experimental SAXS data, flexibility metric of ensemble compared with pool (value in parentheses), ratio of standard deviation for the distribution of selected ensemble to that of the pool, respectively.

separation from PKA using SEC followed by tobacco etch virus (TEV) cleavage, the sample was then evaluated by intact MS, which indicated stoichiometric phosphorylation (Fig. S7, *left panel*), which was also confirmed by western blotting (Fig. S7, *inset right panel*). However, phosphorylation had no effect on the GEF activity of the DH/PH-DEP1 fragment (Fig. 1*B*), nor could the phosphorylated DEP1 domain inhibit the DH/PH module when added in *trans* (Fig. 1*C*). Furthermore, the SEC-SAXS data collected for DH/PH-DEP1 and *p*-DH/PH-DEP1 were nearly indistinguishable (R_g for *p*-DH/PH-DEP1 was 29.6 ± 0.07 Å) as was the EOM analysis (Fig. 3*F*). We had observed that mutation of individual basic residues in the DEP1 hairpin could alter the oligomerization status of the DEP1 domain, as evaluated by SEC (Fig. S2*B*). However, phosphorylation also had no effect on the oligomerization status of the DEP1 domain (data not shown). Thus, stoichiometric PKA phosphorylation had no discernable effect on the activity or the solution state properties of the DH/PH-DEP1 or DEP1 fragments of P-Rex1.

P-Rex1 DEP1 domain binds to anionic lipids in a phosphorylation-dependent manner

Evaluation of the electrostatic potential of the DEP1 domain reveals that it has several positively charged patches on its surface that could interact with negatively charged membrane, most notably the β1–β2 hairpin (Fig. 4*A*). The DEP domains of Epac and Dvl mediate membrane localization (32, 37). Thus, we hypothesized that PKA phosphorylation within the basic hairpin loop of DEP1 could perturb lipid binding. First, lipid overlay assays were performed using MBP-His_6–tagged DEP1 protein by incubating the purified protein on nitrocellulose strips containing spotted lipids and then resolving bound protein by western blot analysis. Initially, assays were performed in 50 mM Tris, pH 7.5, and 150 or 50 mM NaCl, but no protein binding was observed. However, under lower salt conditions (0 mM NaCl), DEP1 bound strongly to phosphatidic acid (PA) and weakly to phosphatidylserine (PS) (Fig. 4*B*, *left panel*). To test whether the hairpin is responsible for binding, all five basic residues (Lys-429/Arg-431/Arg-432/Arg-433/Lys-434) in the hairpin were mutated to alanine (MBP-His_6-$DEP1_{5Ala}$). The resulting protein exhibited complete loss of binding under these conditions (Fig. 4*B*, *right panel*).

We next tested whether PA binding affected the activity of the DH/PH-DEP1 fragment of P-Rex1 in the presence of liposomes containing various amounts of PA. At physiological levels, the concentration of PA is 0.1-0.3 mol % of the total membrane lipids (38) and at that concentration there was no effect on GEF activity. A significant 2- and 4-fold increase in activity was, however, seen at 10 and 50% PA concentration, respectively (Fig. 1*D*), suggesting that negatively charged lipids such as PA do have the ability to activate the GEF activity of the DH/PH-DEP1 fragment.

To quantitatively assess the effects of PKA phosphorylation on the membrane binding of DEP1, we used liposome sedimentation assays. The DEP1 protein was first incubated with large unilamellar vesicles (LUVs) composed of different concentrations of anionic phospholipids (PS and PA) in addition to control LUVs containing PC and PE alone. These assays were conducted with buffer containing 50 mM Tris-HCl, pH 7.5, 150 mM NaCl and at lower salt conditions with 50 mM NaCl. The absence of DEP1 protein in the liposome pellets at 150 mM NaCl relative to the positive control LactC2 (a PS-binding C2 domain from lactadherin) indicated that DEP1 did not bind to either 10% PS or 10% PA containing LUVs at this ionic strength (data not shown). However, at 50 mM NaCl, DEP1 bound as strongly as LactC2 to 10% PA LUVs. Binding was however not evident in the case of *p*-DEP1 (Fig. 4*C*).

Discussion

In this study, we hypothesized that the DEP1 domain plays a key role in mediating autoinhibition in P-Rex1. Comparison of

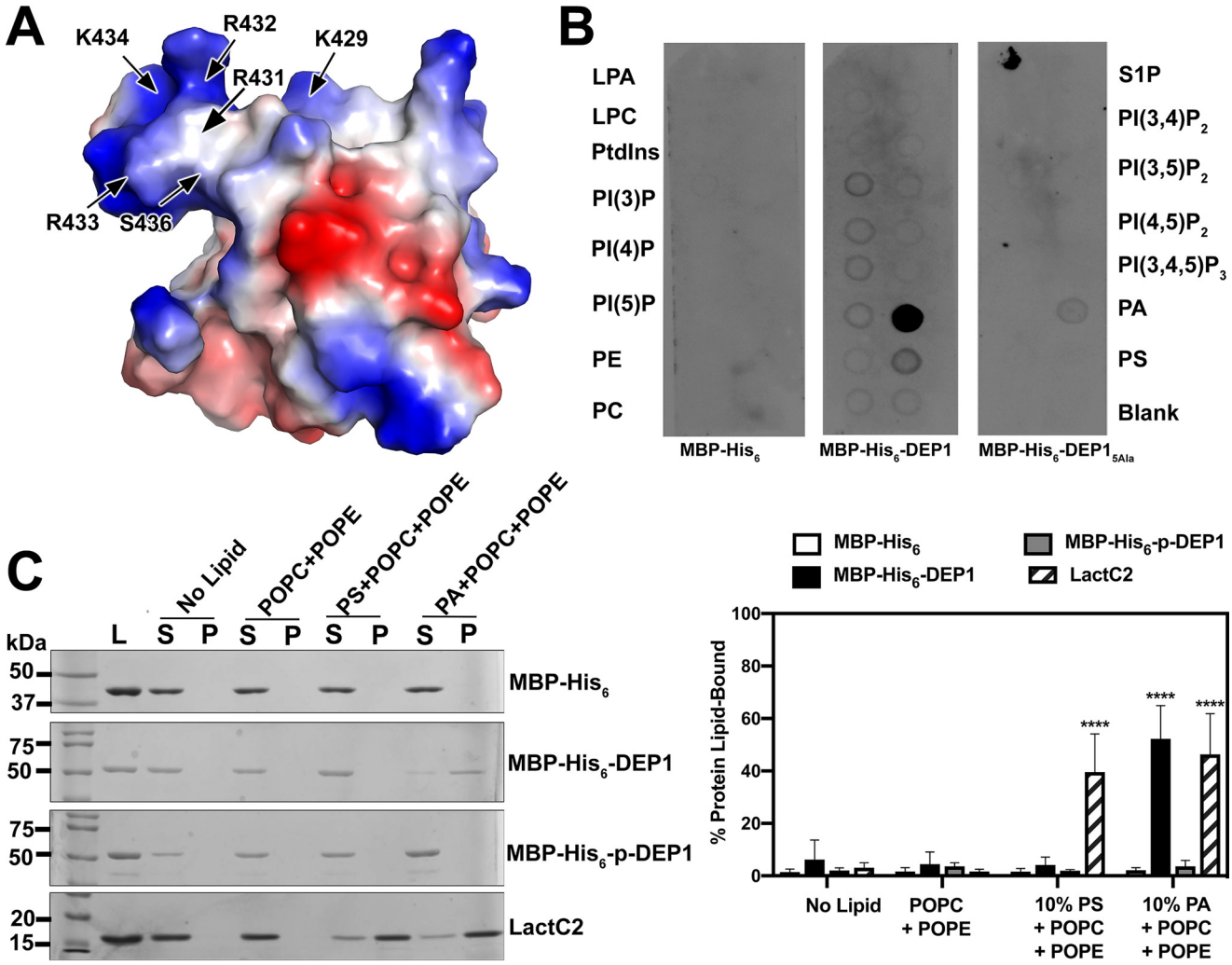

Figure 4. Assessment of the P-Rex1 DEP1 and *p*-DEP1 interaction with lipids. *A,* surface potential of the DEP1 domain. Positively charged residues and PKA phosphorylation site Ser-436 in its β hairpin loop are shown with *arrows*. *Red* and *blue* regions represent negative and positive potential surfaces, respectively. *B,* protein-lipid overlay assays using a PIP strip with 100 pmol of a different lipid per spot incubated with 0.5 mg/ml each of MBP-His_6 (control), MBP-His_6-DEP1, and an alanine mutant (MBP-His_6-$DEP1_{5Ala}$) substituting all five basic residues in its hairpin loop. Protein binding was detected using anti-His-horseradish peroxidase–conjugated antibody. The experiments were performed three times, and a representative result is shown. *LPA*, lysophosphatidic acid; *LPC*, lysophosphatidylcholine; *PI*, phosphatidylinositol. *S1P*, sphingosine-1-phosphate. *C,* binding of DEP1 and *p*-DEP1 to lipid vesicles containing the anionic lipids, PA and PS as measured by the liposome sedimentation assay. 5 μg each of MBP-His_6–tagged DEP1 and *p*-DEP1 proteins, and LactC2 (a His_6–tagged control protein that binds to PS) were incubated with liposomes containing POPC/POPE, POPC/POPE/PS, or POPC/POPE/PA. The control liposome contained 70% POPC, 29% POPE, 1% dansyl-PE. All other liposomes had 10 mol % of PA or PS, compensated with a corresponding decrease in POPE concentration. The binding was evaluated by SDS-PAGE of supernatant (S) and pellet (P) fractions from sedimentation assays (*left panel*). Total protein used is represented by load (*L*). The amount of protein in each fraction was quantitated by densitometry analysis of the corresponding band in SDS-PAGE using ImageJ (*right panel*). Data represent the average of three sedimentation assays, with *error bars* representing the standard deviation of the mean. ****, $p < 0.0001$.

the GEF activities of the DH/PH and DH/PH-DEP1 fragments of P-Rex1 confirmed that DEP1 was autoinhibitory (Fig. 1*B*), in line with cell-based assays wherein P-Rex1 variants that included both DEP1 and DEP2 also exhibited diminished basal GEF activity (15). One straightforward mechanism would be for the DEP1 to interact with the DH domain and block GTPase binding. However, addition of DEP1 in *trans* to the DH/PH module did not inhibit activity, and instead mildly improved it (Fig. 1*C*). If this increase reflects a direct interaction, DEP1 would have to bind to an interface that does not interfere with the GTPase-binding site. The *p*-DEP1 domain gave similar results when added in *trans* to DH/PH (Fig. 1*C*), demonstrating that the putative interaction is not phosphorylation dependent. Direct association of the DEP1 domain with the DH/PH module was further supported by our SEC-SAXS analysis, which determined that the radius of gyration and D_{max} were similar in DH/PH, and DH/PH-DEP1 and thus that the presence of the DEP1 domain, regardless of its phosphorylation status (*i.e.* in *p*-DH/PH-DEP1), stabilized a more compact, less flexible, and less active state.

A direct interaction was also detected between DH/PH and DEP1 in cells by Chavez-Vargas *et al.* (15) by co-immunoprecipitation, although in this case it depended on phosphorylation of DEP1 and correlated with a mild inhibition of membrane-tethered DH/PH GEF activity. Differences with our results may be due to experimental context. For example, it could be that the unphosphorylated DEP1 domain is sequestered in cell lysates by membranes or other electrostatically complementary

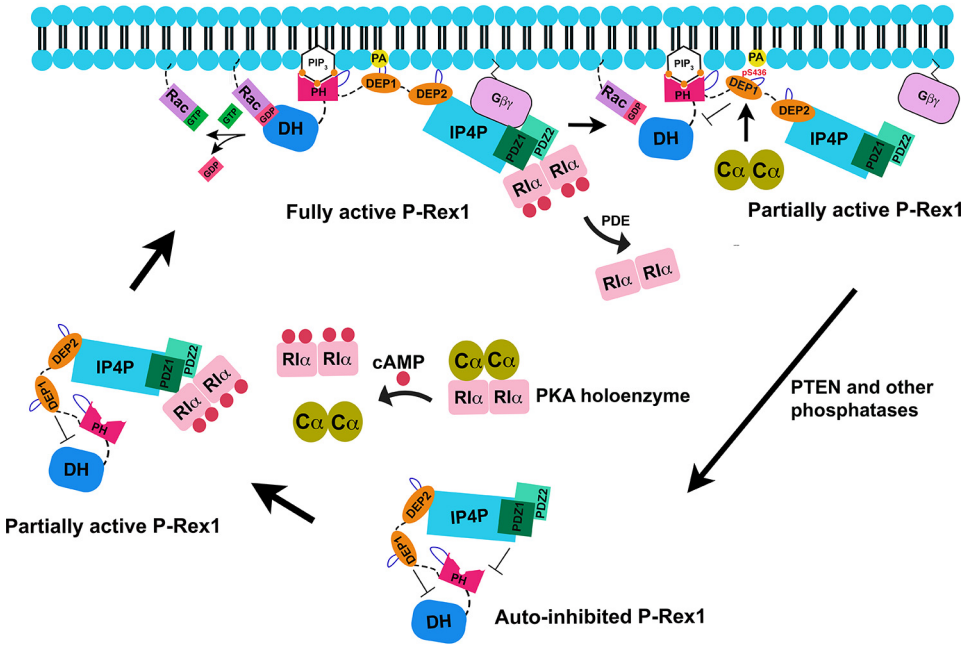

Figure 5. Model of DEP1 mediated inhibition of P-Rex1. Previous biochemical data suggest that the catalytic DH domain of P-Rex1 is autoinhibited in the cytoplasm via its C-terminal domains (*bottom*) (15, 28). Based on the structural data presented here and in prior studies (13), inhibition is likely mediated by both the DEP1 domain and the domains that comprise the Gβγ binding module (DEP2, PDZ1, PDZ2, and IP4P). Activation of GPCRs leads to generation of free Gβγ subunits and production of PIP_3, which help recruit P-Rex1 to the membrane where it adopts an active conformation (*top*). A polybasic stretch within β3–β4 loop of the PH domain (*purple*) is known to promote membrane binding (29), and the basic β1–β2 hairpin loops (also *purple*) in DEP1 and likely DEP2 bind to PA or PS. All three can thus serve as membrane anchors for the activated complex at acidic patches in the membrane, thereby situating P-Rex1 for optimal interactions with Rac1 and helping to relieve autoinhibition. An additional layer of regulation is imposed by PKA. The cAMP-bound Rlα regulatory subunits of type 1 PKA reportedly bind the PDZ1 and PDZ2 domains of P-Rex1, creating a partially active conformation (bottom left) (17). Conversely, the catalytic domains of PKA can phosphorylate Ser-436 (15) within the DEP1 β1–β2 hairpin, lowering the affinity of P-Rex1 for anionic membranes and re-enabling DEP1 to interact with the DH/PH module. This creates another partially active state at the membrane reportedly incompatible with Gβγ binding (*top right*) (14, 16). Oligomerization of P-Rex1 (not shown), perhaps mediated by the DEP1 domain, may confer another layer of regulation. Flexible linkers are shown by *dashed lines*.

surfaces due to its basic hairpin loop. Regardless, the minor effects we and Chavez-Vargas *et al.* (15) observed for DEP1 regulation of GEF activity suggest that the primary mechanism by which phosphorylation of DEP1 by PKA inhibits P-Rex1 is probably distinct from its ability to interact with the DH/PH module.

Our structural analysis suggests other possible modes of DEP1-dependent P-Rex1 regulation. The DEP1 crystal structure exhibited two domain swaps, one involving its β1–β2 hairpin. The β1–β2 hairpin of the Dvl2 DEP domain undergoes a similar domain swap that triggers Dvl2 polymerization and formation of the Wnt signalosome (31). P-Rex1 is also known to form oligomers, at least based on co-immunoprecipitation of GFP- and myc-tagged P-Rex1 (16). Co-association was lost when the N-terminal DH/PH-DEP1 domains were deleted, suggesting that oligomerization is mediated by these N-terminal domains. With this in mind, one of the domain swaps we observed in the P-Rex1 DEP1 crystal structure could regulate P-Rex1 function by promoting dimerization of the enzyme in cells. The context under which this event might occur could further be influenced by PKA phosphorylation. At the very least, the dynamic behavior that must occur at the N terminus of the DEP1 domain in solution would allow the β1–β2 hairpin to extend in a manner that would more efficiently dock to the catalytic domain of PKA.

Because DEP domains are well-known to be involved in membrane targeting (32, 37, 39), we used PIP strip assays to show that DEP1 binds to the negatively charged lipids PA and PS (Fig. 4*A*) and that basic residues in the β1–β2 hairpin are responsible (Fig. 4*B*). Other DEP domains are also responsive to PA (32, 40–41) albeit not always via their β1–β2 hairpin (41). We also showed that PA could increase GEF activity, although at concentrations of PA that are not physiological (Fig. 1*F*). Strikingly, although the DEP1 domain bound to PA-containing liposomes, the PKA-phosphorylated domain did not (Fig. 4*C*). Interestingly, P-Rex1–Ser-436 is analogous to Epac1–Arg-82 (Fig. S1), which is critical for the binding of Epac1 to liposomes containing PA and for cAMP-dependent recruitment of Epac1 to membranes in cells (32). Our data are therefore consistent with PKA phosphorylation inhibiting P-Rex1 activity by eliminating a key membrane binding determinant in P-Rex1, which could hinder the ability of other membrane-localized regulators such as PIP_3 and Gβγ to activate GEF activity (Fig. 5) (14, 16).

Several other signaling proteins are known to selectively bind PA (42–44). These include other GEFs (Sos, DOCK1, DOCK2) and the GTPases Cdc42, Rac1, Arfs-1, -5, and -6. The PH domain of Sos has independent binding sites for $PI(4,5)P_2$ and PA, but PA is what determines its recruitment to the membrane. Similarly, dynamics of DOCK2, a major Rac GEF involved in neutrophil chemotaxis was found to be temporally regulated by $PI(3,4,5)P_3$ and PA. $PI(3,4,5)P_3$ mediated initial translocation to plasma membrane, whereas PA acted in a later phase and stabilized the protein at the leading edge. Although most of the PA-binding proteins have clusters of basic residues in their PA-

binding site, no structural motif selective for PA binding is known, and the DEP1 structure we report also does not give any further insights except that the $\beta1-\beta2$ hairpin is rich in arginine residues. A prior study suggests that in addition to favorable electrostatic interactions between polybasic stretches and negatively charged PA, the guanidinium side chains of arginine residues are particularly important because they can provide two salt bridges with PA, enhancing the selectivity and the strength of the interaction (45). PA clustering also promotes negative curvature on membranes, which also has been proposed to promote selective binding for PA-binding domains (46).

In conclusion, our findings suggest that the DEP1 domain could potentially be involved in several aspects of P-Rex1 regulation: 1) inhibition of basal GEF activity by association with the DH/PH module (Fig. 1); 2) serving as a locus for P-Rex1 oligomerization; 3) localization of the enzyme to regions of the membrane with high concentrations of anionic phospholipids, in particular PA; and 4) efficient phosphorylation by PKA, which hinders the domain from binding lipids. Future studies are needed to further define the mechanism of DEP1-dependent inhibition in cells in the context of full-length P-Rex1. But is there a physiological reason why the DEP1 domain would recognize PA? Temporal production of PA by phospholipase D in response to chemokine stimulation is part of the migration response in leukocytes (47). Polybasic loops, which seem to favor binding to PA, also turn out to be conspicuous in P-Rex1, including one in the $\beta3-\beta4$ loop of the PH domain (29), and one in each of the $\beta1-\beta2$ hairpins of DEP1 (this paper) and DEP2 (13) domains. A polybasic PA selective region is also found at the C terminus of Rac1 (48), the primary substrate of P-Rex1 *in vivo*. Thus, PA production by phospholipase D at the leading edge of leukocytes could act as an organizational signal that promotes the co-localization and interaction of P-Rex1, its substrate Rac1, and perhaps other signaling molecules.

Experimental procedures

Protein expression and purification

DEP1 (residues 409-499) was cloned into expression vector pMCSG9 using ligation independent cloning. DH/PH (residues 38-408) and DH/PH-DEP1 (residues 38-499) were cloned into pMal-His_{10} using restriction cloning. pET15b-PKA Catα was a gift from Dr. Susan Taylor (University of California, San Diego). Site-directed mutagenesis in pMCSG9-DEP1 was performed using QuikChange (Qiagen) and confirmed by DNA sequencing of both strands. All expression constructs were transformed into BL21(DE3). Cells were grown in Terrific Broth at 37 °C until an optical density (OD) of 0.8 was reached following which the temperature was decreased to 18 °C and the cultures were induced with either 0.1 (for P-Rex1 truncation proteins) or 0.4 (for PKA) mM isopropyl 1-thio-β-D-galactopyranoside. The cells were harvested after 16 h, flash frozen, and stored at −80 °C. For DEP1, DH/PH, and PKA proteins, buffer pH 8.0 was used. Buffer pH 7.0 was used for DH/PH-DEP1. The cells were re-suspended in lysis buffer containing 20 mM HEPES, pH 7 or 8, 300 or 100 mM NaCl (P-Rex1 truncation proteins and PKA, respectively), 0.1 M phenylmethylsulfonyl fluoride, 6 μM LL, and 1 mM DTT and lysed using a high pressure Avestin EmulsiFlex-C3. The lysate was centrifuged at 15,000 × *g* for 60 min at 4 °C. The supernatant was then incubated with Ni-NTA resin for 1 h at 4 °C with stirring. For P-Rex1 truncation proteins, the resin was first washed with 50 column volumes (CV) of lysis buffer. Second wash with 50 CV was performed with lysis buffer containing 5, 20, or 25 mM imidazole for DEP1, DH/PH, and DH/PH-DEP1, respectively. The proteins were then eluted with lysis buffer supplemented with 250 mM imidazole. Resin loaded with PKA was first washed with lysis buffer followed by wash buffer containing 20 mM HEPES, pH 8, 500 mM NaCl, and 10 mM imidazole. Another low salt wash with 20 mM HEPES, pH 8, 200 mM NaCl was given before PKA elution in lysis buffer supplemented with 250 mM imidazole. The elution fractions of MBP-His tagged proteins analyzed by SDS-PAGE were pooled and incubated with 2% TEV protease at 4 °C overnight in dialysis buffer (20 mM HEPES, pH 7 or 8, 200 (DEP1) or 300 (DH/PH and DH/PH-DEP1) mM NaCl, 10% glycerol, and 2 mM DTT) to cleave off the MBP-His_6 and MBP-His_{10} tags from DEP1 and DH/PH or DH/PH-DEP1, respectively. Subsequently, cleaved DEP1 was incubated with a re-equilibrated Ni-NTA for 30 min and the flow-through was further purified via SEC on an analytical Superdex S75 column (GE Healthcare) in a running buffer containing 20 mM HEPES, pH 8, 200 mM NaCl, and 2 mM DTT. The eluted DEP1 was concentrated to 35 or 70 mg/ml using a 3-kDa concentrator. The cleaved DH/PH and DH/PH-DEP1 were diluted to 50 mM NaCl in buffer prior to purification on a HiTrap SP-Sepharose column (GE Healthcare) with a gradient of 0.0-1.0 M NaCl at pH 8 and 7, respectively. Collected fractions were run over an analytical S200 SEC column in running buffer (20 mM HEPES, pH 8 or 7, 300 mM NaCl, and 2 mM DTT). Proteins collected from SEC were flash frozen and stored at −80 °C. The pET28a-His_6-LactC2 bacterial expression plasmid was a gift from Dr. Sergio Grinstein (University of Toronto). His_6-LactC2 was expressed and purified as described previously (49). Briefly, protein eluted from a Ni-NTA column (Qiagen) was further purified using SEC on a HiLoad 16/600 Superdex 200 PG column (ÄKTA pure, GE Healthcare). Fractions containing LactC2 were pooled, concentrated, and protein was quantified using the Pierce bicinchoninic acid assay. The protein was stored at 4 °C in storage buffer (10 mM Tris, pH 8, 300 mM NaCl).

Production and MS analysis of DH/PH-DEP1 and p-DH/PH-DEP1

For producing phosphorylated proteins, Ni-NTA purified MBP-His_6-DEP1 and MBP-His_{10}-DH/PH-DEP1 were dialyzed in 20 mM HEPES, pH 8 or 7, 100 mM NaCl, 2 mM DTT and incubated with PKA in the presence of 5 mM $MgCl_2$ and 10 mM ATP for 2 h at 25 °C. The molecular weight difference between MBP-His_{10}, DH/PH-DEP1, and PKA proteins is too small for resolution on SEC, and PKA could not be removed by ion exchange, therefore uncleaved MBP-His_{10}-*p*-DH/PH-DEP1 was passed over an analytical S200 SEC to remove PKA. MBP-His_6-*p*-DEP1 from the kinase reaction and MBP-His_{10}-*p*-DH/PH-DEP1 collected from S200 SEC were cleaved by TEV during dialysis as described above. To remove MBP-His_{10} from

p-DH/PH-DEP1, cleaved protein was diluted to 50 mM NaCl in buffer and subjected to cation exchange via an SP-Sepharose column with a gradient of 0.0-1.0 M NaCl in pH 7. The protein collected from the cation exchange was run over analytical S200 SEC column in 20 mM HEPES pH 7, 300 mM NaCl, and 2 mM DTT. For liposome sedimentation assays, MBP-His_6-*p*-DEP1 after the kinase reaction was directly run over S200 SEC. Proteins from SEC were flash frozen, and kept at −80 °C. For MALDI TOF MS analysis, α-cyano-4-hydroxycinnamic acid purchased from Sigma-Aldrich was used as a matrix and prepared at 1 mg/ml in 50% acetonitrile, 50% water, 0.1% formic acid. The matrix solution was mixed with the protein sample in a ratio of 1:1 (v/v), and 1 μl of the matrix–analyte mix was spotted on a Opti-TOFTM 384 (123 × 81 mm) MALDI plate (MDS-SCIEX) and allowed to dry for 45 min at ambient temperature. The instrument was calibrated using a standard calibration mix obtained from SCIEX that contains six peptides (des-Arg-1-bradykinin, angiotensin, Glu-1-FibB, ACTH(1-17), ACTH(18-39), and ACTH(7-38). To prepare the stock solution of the calibration mix, each vial containing the standard mix was re-suspended in 100 μl of 50% acetonitrile, 50% water, 0.1% formic acid. 1 μl of the calibration mix stock was mixed with 9 μl of α-cyano-4-hydroxycinnamic acid solution and 1 μl was spotted on the Opti-TOFTM 384 MALDI plate. The concentration of the standards ranged from 1 to 3 pmol/μl depending on the peptide.

MS spectra for both DH/PH-DEP1 and *p*-DH/PH-DEP1 were acquired using a 4800 MALDI-TOF/TOF mass spectrometer (Applied Biosystems MDS-SCIEX) analyzer. The instrument was operated under automated, linear-mode acquisition parameters with a method optimized for acquisition at a *m*/*z* of 20,000 to 100,000 using a 200 Hz fixed laser intensity for 1000 shots/spectrum with a uniformly random laser shot pattern. A total of 1000 laser shots were collected for each matrix spot in increments of 50 shots beginning at the center of each spot and randomly rastering at different positions within the spot. Automated profile acquisition required the creation of custom plate geometry files that involved the determination of the relative coordinate of each matrix spot from an optical image of the prepared MALDI plate. Data were processed using 4000 series Explorer software.

Guanine nucleotide exchange assay

A FRET-based assay was used to assess the nucleotide exchange activity of DH/PH, DH/PH-DEP1, and *p*-DH/PH-DEP1 under various conditions. The inhibition (Fig. 1*B*) and competition assays (Fig. 1*C*) were performed in the absence of liposomes. For checking the effect of PA on DH/PH-DEP1 activity, included 100 nM GEF protein was first incubated with liposomes for 20 min at room temperature. Just before measurement, Cdc42 loaded with 2′/3′-*O*-(*N*-methyl-anthraniloyl)-guanosine-5′-diphosphate (MANT-GDP) (Jena Biosciences) in reaction buffer containing 20 mM HEPES, pH 8, 100 mM NaCl, 0.5 mM $MgCl_2$, 100 μM GTP, and 1 mM DTT, was injected to a final concentration of 2 μM in a volume of 100 μl. In competition assays, the protocol was the same as described earlier with exception that increasing concentrations (0-100 μM) of DEP1 or *p*-DEP1 were incubated with DH/PH protein for 20 min at room temperature before initiating the reaction by adding mant-GDP–labeled Cdc42. The mixture was then excited at 360 nm, and the fluorescence intensity at 450 nm was measured in 10-13–s intervals on a Flexstation 3 plate reader for a total of 40 min. Fluorescence curves were then fit to a one-phase exponential association model using GraphPad Prism.

DEP1 crystallization

Crystallization screens were set using a hanging drop diffusion format with 150 nl of reservoir solutions from MIDASplus (Molecular Dimensions) mixed with 150 nl of 70 mg/ml DEP1 protein at 20 °C. Crystals grew with reservoir solution containing 0.1 M HEPES, pH 6.5, 45% (w/v) poly(acrylic acid sodium salt) 2100, and were harvested directly from the screening condition into reservoir solution. Crystals were removed on nylon cryoloops and then plunged into liquid N_2.

Data collection and structure determination

Diffraction data were collected from one crystal on the 23-ID-D beamline at the Advanced Photon Source at Argonne National Laboratory on a Pilatus3 6M detector. Data were reduced, indexed, integrated, and scaled using the HKL3000 software package (50). Initial phases were determined by molecular replacement using CCP4 software package (51) with PDB entry 1O7F as a search model. Initial refinement consisted of model building in Coot alternating with reciprocal space refinement in Refmac (52) using TLS parameters. Diffraction and refinement statistics are described in Table 2. DEP1 coordinates and structure factors have been deposited into the PDB under accession code 6VSK.

Protein-lipid overlay assays

Nitrocellulose membrane strips (number P-6001; Echelon Biosciences) spotted with 100 pmol of various lipids were first blocked with 3% BSA in wash buffer (50 mM Tris-HCl, pH 7.5, 0.05% Tween 20) for 1 h at room temperature followed by incubation with MBP-His_6, MBP-His_6-DEP1, or MBP-His_6-$DEP1_{5Ala}$ at a concentration of 0.5 mg/ml for 2 h at room temperature. The strips were washed three times for 5 min each with buffer and then incubated with anti-histidine horseradish peroxidase-tagged antibody for 1.5 h. To remove unbound antibody, the blot was rinsed three times with wash buffer for 5 min each. Bound protein was detected by chemiluminescence.

Liposome preparation

Liposomes used for GEF assays were composed of phosphatidylethanolamine (PE) (16:0/18:1; number 850757), phosphatidylcholine (PC) (16:0/18:1; number 850457), and varying concentrations of PA (16:0/18:1; number840857) (Avanti Polar Lipids Inc.). The total lipid concentration was 1 mM in liposomes used for analyzing the effect of PA on DH/PH-DEP1 GEF activity (Fig. 1*D*). The ratio of PC:PE was kept at 50%. The liposomes were prepared as 10× stocks by combining liquid chloroform stocks together and then drying the mixture under N_2. The lipid film layer was further desiccated for 2 h before

Table 2
Crystallographic data collection and refinement statistics
Statistics for the highest-resolution shell are shown in parentheses.

	P-Rex 1 DEP1 domain
Wavelength	1.033
Resolution range	19.49-3.12 (3.23-3.12)
Space group	$P6_322$
Unit cell (Å, °)	103 103 70.0 90 90 120
Total reflections	34,606
Unique reflections	4,064 (379)
Multiplicity	19 (1.3)
Completeness (%)	98.5 (94.5)
Mean $I/\sigma(I)$	19 (1.3)
Wilson B-factor	97.7
R_{meas}	0.15 (0.60)
R_{pim}	0.05 (0.32)
$CC_{1/2}$	1 (0.71)
Reflections used in refinement	4,061 (379)
Reflections used for *R*-free	213 (20)
R_{work}	0.228 (0.343)
R_{free}	0.254 (0.386)
Number of nonhydrogen atoms	754
Solvent atoms	4
Protein residues	91
Root mean square (distances)	0.013
Root mean square (angles)	2.10
Ramachandran favored (%)	91.0
Ramachandran allowed (%)	6.70
Ramachandran outliers (%)	2.30
Rotamer outliers (%)	8.6
Clash score	15.9
Average B-factor	79.1
Macromolecule	79.3
Solvent	45.0
Number of TLS groups	1

resuspension in 20 mM HEPES, pH 8, and 100 mM NaCl. The lipid solution was mixed and sonicated in a water bath until it became clear. The liposomes were either used fresh or stored at 4 °C and used within 3 to 4 days of generation. LUVs for liposome sedimentation assays were prepared by combining POPC (1-palmitoyl-2-oleoyl-glycero-3-phosphocholine), POPE (1-palmitoyl-2-oleoyl-*sn*-glycero-phosphoethanolamine), and dansyl-PE (1,2-dioleoyl-*sn*-glycero-3-phosphoethanolamine-*N*-(5-dimethylamino-1-naphthalenesulfonyl) (ammonium salt) with either PS or PA, as indicated. Control vesicles containing only POPC, POPE, and dansyl-PE contained these lipids at a final mol % of 70, 29, and 1, respectively. Addition of 10% PS or 10% PA in the anionic lipid vesicles was compensated by decreasing POPE by 10%, whereas POPC and dansyl-PE were held constant. Chloroform-solubilized stock lipids were mixed to yield the various vesicle compositions and dried into a film under a steady stream of N_2. Lipid films were stored at −20 °C. On the day of the experiment, lipid films were hydrated in extrusion buffer (250 mM raffinose pentahydrate, 25 mM Tris, pH 7.5, 1 mM DTT) for 1 h at 37 °C, vortexing every 15 min. Rehydrated lipids were extruded 15 times through a 200-nm Whatman polycarbonate filter (GE Healthcare) to form LUVs. LUVs were diluted in 3× volume with the appropriate 1× binding buffer (normal conditions: 25 mM Tris, pH 7.5, 1 mM DTT, 0.5 mM EDTA, 150 mM NaCl; reduced salt conditions: 25 mM Tris, 1 mM DTT, 0.5 mM EDTA, 50 mM NaCl, pH 7.5).

Liposome sedimentation assays

Liposome sedimentation assays were performed as previously described (53). Briefly, proteins were centrifuged at 16,000 × *g* for 5 min to remove any precipitate. Equal volumes of clarified protein (5 μg) and re-suspended LUV (final concentration = 2 mM) were incubated for 30 min on an orbital shaker at room temperature and then centrifuged at 50,000 × *g* for 30 min at 22°C. Using a UV lamp to visualize the fluorescent LUV pellet, the supernatant containing unbound protein was removed carefully without disrupting the pellet and transferred into a clean Eppendorf tube. The supernatant was diluted with 0.4× volume of 6× denaturing SDS-PAGE loading dye. The pellet was washed by resuspending in 12× volume of the appropriate 1× binding buffer. The resuspended pellet was transferred to a fresh tube and centrifuged at 16,000 × *g* for 30 min at 22°C. Again, using the UV lamp, the supernatant was carefully removed but this time discarded. The washed pellet was resuspended in 1.2× volume of 1× denaturing SDS-PAGE loading dye. Equal volumes of supernatant and pellet samples were resolved on a 10% SDS-PAGE gel and protein content was visualized using Coomassie Brilliant Blue staining. A GE Amersham Biosciences 600 imager was used to collect a high-resolution tiff image of each gel that was analyzed with densitometry analysis in ImageJ. To calculate % protein bound the following equation was used: $density_{pellet}/density_{total}$, where $density_{total} = 2(density_{supernatant}) + density_{pellet}$.

SEC-SAXS

SEC-SAXS was performed at the BioCAT beamline (Sector 18) at the Advanced Photon Source, Argonne National Laboratory equipped with an AKTA Pure FPLC and a Pilatus3 X 1M detector. Purified proteins (DH/PH, DH/PH-DEP1, and *p*-DH/PH-DEP1) were injected onto a Superdex 200 Increase 10/300 column at a final concentration of 5 mg/ml in 20 mM HEPES, pH 8, 300 mM NaCl for DH/PH and 20 mM HEPES, pH 7, 300 mM NaCl for DH/PH-DEP1 and *p*-DH/PH-DEP1). Samples were centrifuged at 16,000 × *g* for 5 min at 4 °C prior to data collection. The eluate from the SEC column flowed through a UV monitor into SAXS flow cell. Scattering data were collected at room temperature using 12 KeV X-rays (1.033 Å wavelength) and 3.67 m sample-to-detector distance. Data were collected every 1 s with 0.5-s exposure times. The achievable q range for this experimental setup was (0.0043-0.3546 $Å^{-1}$).

SEC-SAXS data processing and analysis

Scattering data were reduced and processed using BioXTAS RAW 1.6.3 (54) software, including azimuthal averaging, buffer subtraction, and averaging of subtracted frames in the elution peak. Buffer subtraction was done using pre-peak buffer. The same program was used to find the forward scattering I(0) and the radius of gyration, R_g via Guinier analysis and molecular weight was determined by both the adjusted Porod volume and volume of correlation methods (34, 55). The pair distance distribution function P(r) was calculated using the indirect Fourier transformation method implemented in GNOM (56) from the ATSAS 2.8.4 package (57). The P(r) function analysis also provided the maximum particle dimension of the protein and an alternative calculation of R_g I(0). Normalized Kratky plots suggested a significant degree of flexibility in the samples. To evaluate the degree of conformational dynamics and flexibility, EOM analysis was carried out on all three proteins (DH/PH,

DH/PH-DEP1, and *p*-DH/PH-DEP1) using the EOM 2.0 program from ATSAS 2.8.4. EOM (36) generates a pool of diverse models using information of protein's 3D structure and its sequence. Known crystallographic coordinates from the DH/PH crystal structure (PDB 5FI1) and DEP1 coordinates (this paper) were kept fixed, and the program generated random configurations of a Cα trace based on sequence for the unknown regions. For DH/PH the first 45 residues, a six-residue linker from 242 to 246, a loop from 305 to 323, and C-terminal residues after 407 were left flexible. For DH/PH-DEP1 the same residues were left flexible, as was the 4-amino acid linker from the PH domain to DEP1 and the 4-amino acid C-terminal tail of DEP1. EOM was used to generate 50,000 possible profiles for the full pool using default settings and native-like structures. A subensemble that matches the scattering data is then selected by a genetic algorithm run 10 times using default settings to verify the stability of the results (results from 1 run are shown in Fig. 3). Results of the SAXS analysis are presented in accordance with the revised guidelines for publishing SAXS data (58). The SAXS data are deposited in SASBD (https://www.sasbdb.org/) with access codes SASDHY9, SASDHW9, SASDHX9, for DH/PH, DH/PH-DEP1, and *p*-DH/PH-DEP1, respectively.

Statistical analysis

Statistical analyses of GEF activity assays were performed using GraphPad Prism 7 software (GraphPad Software Inc., La Jolla, CA) on data from three or more independent experiments measured in duplicate. To evaluate the significance of difference between the GEF activities one-way analysis of variance was carried out. Error bars represent S.D. The liposome sedimentation assays were done in replicates and data from three independent experiments data were used to measure standard deviation of the mean. The data were statistically analyzed using Dunnett's multiple comparison test.

Data availability

Data not provided within the manuscript is available upon reasonable request. Structure factor amplitudes for the DEP1 structure are deposited in the Protein Data Bank with access code 6VSK. The SAXS data for DH/PH, DH/PH-DEP1, and *p*-DH/PH-DEP1, is deposited in SASBDB with access codes SASDHY9, SASDHW9, and SASDHX9 respectively.

Acknowledgments—We thank Dr. Srinivas Chakravarthy, Beamline Scientist, for performing the SEC-SAXS at BioCAT, Chicago, IL, Dr. Yu-Chen Yen for help in X-ray crystallography data processing, Dr. Qiuyan Chen for scientific discussions, and Dr. Larisa V. Avramova for technical support. We are grateful to Purdue Proteomics Facility, Bindley Bioscience Center, Purdue University for MALDI TOF-MS data collection and analysis. We thank Victoria Hedrick and Dr. Uma Aryal of the Purdue Proteomics Facility for their help with MALDI TOF-MS analysis. GM/CA@APS was supported in whole or in part with federal funds from National Cancer Institute Grant ACB-12002 and the National Institute of General Medical Sciences Grant AGM-12006. BioCAT was supported by National Institutes of Health NIGMS Grant 9 P41 GM103622. Use of the Pilatus 3 1M detector was provided by NIGMS Grant 1S10OD018090-01. This research used resources of the Advanced Photon Source, a U.S. Department of Energy (DOE) Office of Science User Facility operated for the DOE Office of Science by Argonne National Laboratory under Contract No. DE-AC02-06CH11357.

Author contributions—S. K. R. and J. J. T. conceptualization; S. K. R., J. B. H., C. B. P., and R. V. S. formal analysis; S. K. R., J. B. H., and C. B. P. validation; S. K.R., J. B. H., C. B. P., S. R. A., M. A. K., and R. V. S. investigation; S. K. R. and J. B. H. visualization; S. K. R., J. B. H., C. B. P., R. V. S., and J. J. T. methodology; S. K. R., J. B. H., C. B. P., and J. J. T. writing-original draft; S. K. R., J. N. C., R. V. S., and J. J. T. writing-review and editing; J. N. C. and R. V. S. resources; J. N. C., R. V. S., and J. J. T. supervision; R. V. S. and J. J. T. funding acquisition; J. J. T. project administration.

Funding and additional information—This work was supported by National Institutes of Health Grants CA221289, HL122416, HL071818 (to J. J. G. T.), and GM131352 (to R. V. S.) and a grant from the Walther Cancer Foundation (to J. J. G. T.). S. R. A. and M. A. K. were recipients of Summer Undergraduate Research Fellowships (SURF) supported by Purdue University. The content is solely the responsibility of the authors and does not necessarily represent the official views of the National Institutes of Health.

Conflict of interest—The authors declare that they have no conflicts of interest with the contents of this article.

Abbreviations—The abbreviations used are: Dbl, diffuse B cell lymphoma; GEF, guanine nucleotide exchange factor; DH, Dbl homology; PH, pleckstrin homology; SH3, Src-homology 3; PIP_3, phosphatidylinositol (3,4,5)-trisphosphate; P-Rex1, PIP_3-dependent Rac exchanger 1; IP4P, inositol polyphosphate-4-phosphatase; GPCR, G protein–coupled receptor; SEC, size exclusion chromatography; PKA, protein kinase A; EOM, ensemble optimization method; PA, phosphatidic acid; PS, phosphatidylserine; LUV, large unilamellar vesicle; Ni-NTA, nickel-nitrilotriacetic acid; CV, column volume; TEV, tobacco etch virus; PE, phosphatidylethanolamine; PC, phosphatidylcholine; POPC, 1-palmitoyl-2-oleoyl-glycero-3-phosphocholine; POPE, 1-palmitoyl-2-oleoyl-s*n*-glycero-phosphoethanolamine; dansyl-PE, 1,2-dioleoyl-s*n*-glycero-3-phosphoethanolamine-*N*-(5-dimethylamino-1-naphthalenesulfonyl).

References

1. Eva, A., Vecchio, G., Rao, C. D., Tronick, S. R., and Aaronson, S. A. (1988) The predicted DBL oncogene product defines a distinct class of transforming proteins. *Proc. Natl. Acad. Sci. U.S.A.* **85,** 2061–2065 CrossRef Medline
2. Rossman, K. L., Der, C. J., and Sondek, J. (2005) GEF means go: turning on RHO GTPases with guanine nucleotide-exchange factors. *Nat. Rev. Mol. Cell Biol.* **6,** 167–180 CrossRef Medline
3. Cook, D. R., Rossman, K. L., and Der, C. J. (2014) Rho guanine nucleotide exchange factors: regulators of Rho GTPase activity in development and disease. *Oncogene* **33,** 4021–4035 CrossRef Medline
4. Stam, J. C., Sander, E. E., Michiels, F., van Leeuwen, F. N., Kain, H. E., van der Kammen, R. A., and Collard, J. G. (1997) Targeting of Tiam1 to the plasma membrane requires the cooperative function of the N-terminal pleckstrin homology domain and an adjacent protein interaction domain. *J. Biol. Chem.* **272,** 28447–28454 CrossRef Medline
5. Whitehead, I., Kirk, H., Tognon, C., Trigo-Gonzalez, G., and Kay, R. (1995) Expression cloning of lfc, a novel oncogene with structural

similarities to guanine nucleotide exchange factors and to the regulatory region of protein kinase C. *J. Biol. Chem.* **270,** 18388–18395 CrossRef Medline
6. Bellanger, J. M., Astier, C., Sardet, C., Ohta, Y., Stossel, T. P., and Debant, A. (2000) The Rac1- and RhoG-specific GEF domain of Trio targets filamin to remodel cytoskeletal actin. *Nat. Cell Biol.* **2,** 888–892 CrossRef Medline
7. Lutz, S., Shankaranarayanan, A., Coco, C., Ridilla, M., Nance, M. R., Vettel, C., Baltus, D., Evelyn, C. R., Neubig, R. R., Wieland, T., and Tesmer, J. J. (2007) Structure of $G\alpha_q$-p63RhoGEF-RhoA complex reveals a pathway for the activation of RhoA by GPCRs. *Science* **318,** 1923–1927 CrossRef Medline
8. Bandekar, S. J., Arang, N., Tully, E. S., Tang, B. A., Barton, B. L., Li, S., Gutkind, J. S., and Tesmer, J. J. G. (2019) Structure of the C-terminal guanine nucleotide exchange factor module of Trio in an autoinhibited conformation reveals its oncogenic potential. *Sci. Signal.* **12,** eaav2449 CrossRef Medline
9. Rossman, K. L., Worthylake, D. K., Snyder, J. T., Siderovski, D. P., Campbell, S. L., and Sondek, J. (2002) A crystallographic view of interactions between Dbs and Cdc42: PH domain-assisted guanine nucleotide exchange. *EMBO J.* **21,** 1315–1326 CrossRef Medline
10. Kristelly, R., Gao, G., and Tesmer, J. J. (2004) Structural determinants of RhoA binding and nucleotide exchange in leukemia-associated Rho guanine-nucleotide exchange factor. *J. Biol. Chem.* **279,** 47352–47362 CrossRef Medline
11. Mitin, N., Betts, L., Yohe, M. E., Der, C. J., Sondek, J., and Rossman, K. L. (2007) Release of autoinhibition of ASEF by APC leads to CDC42 activation and tumor suppression. *Nat. Struct. Mol. Biol.* **14,** 814–823 CrossRef Medline
12. Welch, H. C., Coadwell, W. J., Ellson, C. D., Ferguson, G. J., Andrews, S. R., Erdjument-Bromage, H., Tempst, P., Hawkins, P. T., and Stephens, L. R. (2002) P-Rex1, a PtdIns(3,4,5)P3- and $G\beta\gamma$-regulated guanine-nucleotide exchange factor for Rac. *Cell* **108,** 809–821 CrossRef Medline
13. Cash, J. N., Urata, S., Li, S., Ravala, S. K., Avramova, L. V., Shost, M. D., Gutkind, J. S., Tesmer, J. J. G., and Cianfrocco, M. A. (2019) Cryo-electron microscopy structure and analysis of the P-Rex1-$G\beta\gamma$ signaling scaffold. *Sci. Adv.* **5,** eaax8855 CrossRef Medline
14. Mayeenuddin, L. H., and Garrison, J. C. (2006) Phosphorylation of P-Rex1 by the cyclic AMP-dependent protein kinase inhibits the phosphatidylinositiol (3,4,5)-trisphosphate and $G\beta\gamma$-mediated regulation of its activity. *J. Biol. Chem.* **281,** 1921–1928 CrossRef Medline
15. Chávez-Vargas, L., Adame-Garcia, S. R., Cervantes-Villagrana, R. D., Castillo-Kauil, A., Bruystens, J. G., Fukuhara, S., Taylor, S. S., Mochizuki, N., Reyes-Cruz, G., and Vázquez-Prado, J. (2016) Protein kinase A (PKA) type I interacts with P-Rex1, a Rac guanine nucleotide exchange factor: effect on PKA localization and P-Rex1 signaling. *J. Biol. Chem.* **291,** 6182–6199 CrossRef Medline
16. Urano, D., Nakata, A., Mizuno, N., Tago, K., and Itoh, H. (2008) Domain-domain interaction of P-Rex1 is essential for the activation and inhibition by G protein $\beta\gamma$ subunits and PKA. *Cell Signal.* **20,** 1545–1554 CrossRef Medline
17. Adame-Garcia, S. R., Cervantes-Villagrana, R. D., Orduñna-Castillo, L. B., Del Rio, J. C., Gutkind, J. S., Reyes-Cruz, G., Taylor, S. S., and Vázquez-Prado, J. (2019) cAMP-dependent activation of the Rac guanine exchange factor P-REX1 by type I protein kinase A (PKA) regulatory subunits. *J. Biol. Chem.* **294,** 2232–2246 CrossRef Medline
18. Lawson, C. D., Donald, S., Anderson, K. E., Patton, D. T., and Welch, H. C. (2011) P-Rex1 and Vav1 cooperate in the regulation of formyl-methionyl-leucyl-phenylalanine-dependent neutrophil responses. *J. Immunol.* **186,** 1467–1476 CrossRef Medline
19. Naikawadi, R. P., Cheng, N., Vogel, S. M., Qian, F., Wu, D., Malik, A. B., and Ye, R. D. (2012) A critical role for phosphatidylinositol (3,4,5)-trisphosphate-dependent Rac exchanger 1 in endothelial junction disruption and vascular hyperpermeability. *Circ. Res.* **111,** 1517–1527 CrossRef Medline
20. Yoshizawa, M., Kawauchi, T., Sone, M., Nishimura, Y. V., Terao, M., Chihama, K., Nabeshima, Y., and Hoshino, M. (2005) Involvement of a Rac activator, P-Rex1, in neurotrophin-derived signaling and neuronal migration. *J. Neurosci.* **25,** 4406–4419 CrossRef Medline
21. Sosa, M. S., Lopez-Haber, C., Yang, C., Wang, H., Lemmon, M. A., Busillo, J. M., Luo, J., Benovic, J. L., Klein-Szanto, A., Yagi, H., Gutkind, J. S., Parsons, R. E., and Kazanietz, M. G. (2010) Identification of the Rac-GEF P-Rex1 as an essential mediator of ErbB signaling in breast cancer. *Mol. Cell* **40,** 877–892 CrossRef Medline
22. Qin, J., Xie, Y., Wang, B., Hoshino, M., Wolff, D. W., Zhao, J., Scofield, M. A., Dowd, F. J., Lin, M. F., and Tu, Y. (2009) Upregulation of PIP3-dependent Rac exchanger 1 (P-Rex1) promotes prostate cancer metastasis. *Oncogene* **28,** 1853–1863 CrossRef Medline
23. Lindsay, C. R., Lawn, S., Campbell, A. D., Faller, W. J., Rambow, F., Mort, R. L., Timpson, P., Li, A., Cammareri, P., Ridgway, R. A., Morton, J. P., Doyle, B., Hegarty, S., Rafferty, M., Murphy, I. G., *et al.* (2011) P-Rex1 is required for efficient melanoblast migration and melanoma metastasis. *Nat. Commun.* **2,** 555 CrossRef Medline
24. Li, J., Chai, A., Wang, L., Ma, Y., Wu, Z., Yu, H., Mei, L., Lu, L., Zhang, C., Yue, W., Xu, L., Rao, Y., and Zhang, D. (2015) Synaptic P-Rex1 signaling regulates hippocampal long-term depression and autism-like social behavior. *Proc. Natl. Acad. Sci. U.S.A.* **112,** E6964–E6972 CrossRef Medline
25. Liang, Q., Cheng, N., Zhang, G., Liang, Y., Qian, F., Wu, D., and Ye, R. D. (2016) Identification of P-Rex1 as an anti-inflammatory and anti-fibrogenic target for pulmonary fibrosis. *Sci. Rep.* **6,** 25785 CrossRef Medline
26. Lewis, J. P., Palmer, N. D., Ellington, J. B., Divers, J., Ng, M. C., Lu, L., Langefeld, C. D., Freedman, B. I., and Bowden, D. W. (2010) Analysis of candidate genes on chromosome 20q12-13.1 reveals evidence for BMI mediated association of PREX1 with type 2 diabetes in European Americans. *Genomics* **96,** 211–219 CrossRef Medline
27. Barrows, D., He, J. Z., and Parsons, R. (2016) PREX1 protein function is negatively regulated downstream of receptor tyrosine kinase activation by p21-activated kinases (PAKs). *J. Biol. Chem.* **291,** 20042–20054 CrossRef Medline
28. Hill, K., Krugmann, S., Andrews, S. R., Coadwell, W. J., Finan, P., Welch, H. C., Hawkins, P. T., and Stephens, L. R. (2005) Regulation of P-Rex1 by phosphatidylinositol (3,4,5)-trisphosphate and $G\beta\gamma$ subunits. *J. Biol. Chem.* **280,** 4166–4173 CrossRef Medline
29. Cash, J. N., Davis, E. M., and Tesmer, J. J. (2016) Structural and biochemical characterization of the catalytic core of the metastatic factor P-Rex1 and its regulation by PtdIns(3,4,5)P3. *Structure* **24,** 730–740 CrossRef Medline
30. Hernández-Negrete, I., Carretero-Ortega, J., Rosenfeldt, H., Hernández-García, R., Calderón-Salinas, J. V., Reyes-Cruz, G., Gutkind, J. S., and Vázquez-Prado, J. (2007) P-Rex1 links mammalian target of rapamycin signaling to Rac activation and cell migration. *J. Biol. Chem.* **282,** 23708–23715 CrossRef Medline
31. Gammons, M. V., Renko, M., Johnson, C. M., Rutherford, T. J., and Bienz, M. (2016) Wnt signalosome assembly by DEP domain swapping of Dishevelled. *Mol. Cell* **64,** 92–104 CrossRef Medline
32. Consonni, S. V., Gloerich, M., Spanjaard, E., and Bos, J. L. (2012) cAMP regulates DEP domain-mediated binding of the guanine nucleotide exchange factor Epac1 to phosphatidic acid at the plasma membrane. *Proc. Natl. Acad. Sci. U.S.A.* **109,** 3814–3819 CrossRef Medline
33. Consonni, S. V., Maurice, M. M., and Bos, J. L. (2014) DEP domains: structurally similar but functionally different. *Nat. Rev. Mol. Cell Biol.* **15,** 357–362 CrossRef Medline
34. Rambo, R. P., and Tainer, J. A. (2013) Accurate assessment of mass, models and resolution by small-angle scattering. *Nature* **496,** 477–481 CrossRef Medline
35. Durand, D., Vivès, C., Cannella, D., Pérez, J., Pebay-Peyroula, E., Vachette, P., and Fieschi, F. (2010) NADPH oxidase activator p67(phox) behaves in solution as a multidomain protein with semi-flexible linkers. *J. Struct. Biol.* **169,** 45–53 CrossRef Medline
36. Tria, G., Mertens, H. D., Kachala, M., and Svergun, D. I. (2015) Advanced ensemble modelling of flexible macromolecules using X-ray solution scattering. *IUCr J.* **2,** 207–217 CrossRef Medline
37. Pan, W. J., Pang, S. Z., Huang, T., Guo, H. Y., Wu, D., and Li, L. (2004) Characterization of function of three domains in dishevelled-1: DEP

domain is responsible for membrane translocation of dishevelled-1. *Cell Res* **14,** 324–330 CrossRef Medline
38. Guan, X. L., Cestra, G., Shui, G., Kuhrs, A., Schittenhelm, R. B., Hafen, E., van der Goot, F. G., Robinett, C. C., Gatti, M., Gonzalez-Gaitan, M., and Wenk, M. R. (2013) Biochemical membrane lipidomics during *Drosophila* development. *Dev. Cell* **24,** 98–111 CrossRef Medline
39. Martemyanov, K. A., Lishko, P. V., Calero, N., Keresztes, G., Sokolov, M., Strissel, K. J., Leskov, I. B., Hopp, J. A., Kolesnikov, A. V., Chen, C. K., Lem, J., Heller, S., Burns, M. E., and Arshavsky, V. Y. (2003) The DEP domain determines subcellular targeting of the GTPase activating protein RGS9 *in vivo*. *J. Neurosci.* **23,** 10175–10181 CrossRef Medline
40. Yoon, M. S., Rosenberger, C. L., Wu, C., Truong, N., Sweedler, J. V., and Chen, J. (2015) Rapid mitogenic regulation of the mTORC1 inhibitor, DEPTOR, by phosphatidic acid. *Mol. Cell* **58,** 549–556 CrossRef Medline
41. Capelluto, D. G., Zhao, X., Lucas, A., Lemkul, J. A., Xiao, S., Fu, X., Sun, F., Bevan, D. R., and Finkielstein, C. V. (2014) Biophysical and molecular-dynamics studies of phosphatidic acid binding by the Dvl-2 DEP domain. *Biophys. J.* **106,** 1101–1111 CrossRef Medline
42. Stace, C. L., and Ktistakis, N. T. (2006) Phosphatidic acid- and phosphatidylserine-binding proteins. *Biochim. Biophys. Acta* **1761,** 913–926 CrossRef Medline
43. Jang, J. H., Lee, C. S., Hwang, D., and Ryu, S. H. (2012) Understanding of the roles of phospholipase D and phosphatidic acid through their binding partners. *Prog. Lipid Res.* **51,** 71–81 CrossRef Medline
44. Sanematsu, F., Nishikimi, A., Watanabe, M., Hongu, T., Tanaka, Y., Kanaho, Y., Côté, J. F., and Fukui, Y. (2013) Phosphatidic acid-dependent recruitment and function of the Rac activator DOCK1 during dorsal ruffle formation. *J. Biol. Chem.* **288,** 8092–8100 CrossRef Medline
45. Kooijman, E. E., Tieleman, D. P., Testerink, C., Munnik, T., Rijkers, D. T., Burger, K. N., and de Kruijff, B. (2007) An electrostatic/hydrogen bond switch as the basis for the specific interaction of phosphatidic acid with proteins. *J. Biol. Chem.* **282,** 11356–11364 CrossRef Medline
46. Putta, P., Rankenberg, J., Korver, R. A., van Wijk, R., Munnik, T., Testerink, C., and Kooijman, E. E. (2016) Phosphatidic acid binding proteins display differential binding as a function of membrane curvature stress and chemical properties. *Biochim. Biophys. Acta* **1858,** 2709–2716 CrossRef Medline
47. Momoi, Y., Nishikimi, A., Du, G., Kataoka, T., and Katagiri, K. (2020) Phosphatidic acid regulates subcellular distribution of RA-GEFs critical for chemokine-dependent migration. *Biochem. Biophys. Res. Commun.* **524,** 325–331 CrossRef Medline
48. Chae, Y. C., Kim, J. H., Kim, K. L., Kim, H. W., Lee, H. Y., Heo, W. D., Meyer, T., Suh, P. G., and Ryu, S. H. (2008) Phospholipase D activity regulates integrin-mediated cell spreading and migration by inducing GTP-Rac translocation to the plasma membrane. *Mol. Biol. Cell* **19,** 3111–3123 CrossRef Medline
49. Yeung, T., Gilbert, G. E., Shi, J., Silvius, J., Kapus, A., and Grinstein, S. (2008) Membrane phosphatidylserine regulates surface charge and protein localization. *Science* **319,** 210–213 CrossRef Medline
50. Minor, W., Cymborowski, M., Otwinowski, Z., and Chruszcz, M. (2006) HKL-3000: the integration of data reduction and structure solution–from diffraction images to an initial model in minutes. *Acta Crystallogr. D Biol. Crystallogr.* **62,** 859–866 CrossRef Medline
51. Winn, M. D., Ballard, C. C., Cowtan, K. D., Dodson, E. J., Emsley, P., Evans, P. R., Keegan, R. M., Krissinel, E. B., Leslie, A. G., McCoy, A., McNicholas, S. J., Murshudov, G. N., Pannu, N. S., Potterton, E. A., Powell, H. R., *et al.* (2011) Overview of the CCP4 suite and current developments. *Acta Crystallogr. D Biol. Crystallogr.* **67,** 235–242 CrossRef Medline
52. Murshudov, G. N., Vagin, A. A., and Dodson, E. J. (1997) Refinement of macromolecular structures by the maximum-likelihood method. *Acta Crystallogr. D Biol. Crystallogr.* **53,** 240–255 CrossRef Medline
53. Julkowska, M. M., Rankenberg, J. M., and Testerink, C. (2013) Liposome-binding assays to assess specificity and affinity of phospholipid-protein interactions. *Methods Mol. Biol.* **1009,** 261–271 CrossRef Medline
54. Hopkins, J. B., Gillilan, R. E., and Skou, S. (2017) improvements to a free open-source program for small-angle X-ray scattering data reduction and analysis. *J. Appl. Crystallogr.* **50,** 1545–1553 CrossRef Medline
55. Piiadov, V., Ares de Araújo, E., Oliveira Neto, M., Craievich, A. F., and Polikarpov, I. (2019) SAXSMoW 2.0: online calculator of the molecular weight of proteins in dilute solution from experimental SAXS data measured on a relative scale. *Protein Sci.* **28,** 454–463 CrossRef Medline
56. Svergun, D. I. (1992) Determination of the regularization parameter in indirect-transform methods using perceptual criteria. *J. Appl. Crystallogr.* **25,** 495–503 CrossRef
57. Franke, D., Petoukhov, M. V., Konarev, P. V., Panjkovich, A., Tuukkanen, A., Mertens, H. D. T., Kikhney, A. G., Hajizadeh, N. R., Franklin, J. M., Jeffries, C. M., and Svergun, D. I. (2017) A comprehensive data analysis suite for small-angle scattering from macromolecular solutions. *J. Appl. Crystallogr.* **50,** 1212–1225 CrossRef Medline
58. Trewhella, J., Duff, A. P., Durand, D., Gabel, F., Guss, J. M., Hendrickson, W. A., Hura, G. L., Jacques, D. A., Kirby, N. M., Kwan, A. H., Pérez, J., Pollack, L., Ryan, T. M., Sali, A., Schneidman-Duhovny, D., *et al.* (2017) 2017 publication guidelines for structural modelling of small-angle scattering data from biomolecules in solution: an update. *Acta Crystallogr. D Struct. Biol.* **73,** 710–728 CrossRef Medline